Drug Design, Development and Therapy

Dovepress
Taylor & Francis Group

Open Access Full Text Article

ORIGINAL RESEARCH

Single-Cell Transcriptomics Reveals Riluzole as an Osteoarthritis Candidate Drug via OB-NE Signaling Modulation and CTSS/NOS1 Inhibition

Kun Liu[1], Jia-Li Li[1], Yan Chen[2], Yu-Xin Li[1], Jeffrey D Deng[3], Yun Gong[4], Chong Cao[1], Qin Zeng[1], Zheng-Wu Xiao[5], Kai-Zhi Wen[5], Xiao-Chao Qu[1], Xiang-Ding Chen[1], Yun Deng[6], Hong-Wen Deng[4], Li-Jun Tan[1]

[1]Laboratory of Molecular and Statistical Genetics, College of Life Sciences, Hunan Normal University, Changsha, Hunan, 410081, People's Republic of China; [2]Xingtai Medical College, Xingtai City, Hebei, 054000, People's Republic of China; [3]Geisel School of Medicine, Dartmouth College, Hanover, NH, 03755, USA; [4]Tulane Center of Biomedical Informatics and Genomics, Deming Department of Medicine, Tulane University School of Medicine, New Orleans, LA, 70112, USA; [5]Center for System Biology, Data Sciences, and Reproductive Health, School of Basic Medical Science, Central South University, Changsha, Hunan, 410013, People's Republic of China; [6]Zebrafish Genetics Laboratory, College of Life Sciences, Hunan Normal University, Changsha, 410081, People's Republic of China

Correspondence: Li-Jun Tan, Laboratory of Molecular and Statistical Genetics, College of Life Sciences, Hunan Normal University, Changsha, Hunan, 410081, People's Republic of China, Tel +86-731-8887-2791, Email ljtan@hunnu.edu.cn; Hong-Wen Deng, Tulane Center of Biomedical Informatics and Genomics, Deming Department of Medicine, Tulane University School of Medicine, 1440 Canal Street Suite 1610, New Orleans, LA, 70112, USA, Tel +1 504-988-1310, Email hdeng2@tulane.edu

Introduction: Osteoarthritis (OA) is a degenerative joint disease involving multiple cell types, yet the role of osteoblast (OB)-immune cell interactions remains poorly understood.

Methods: Single-cell RNA sequencing of human femoral head tissue was employed in this study, followed by integrated analysis using bioinformatics tools such as differential expression analysis, enrichment analysis and cell communication analysis. A network proximity-based drug repositioning approach was employed to identify potential drug candidates. Mendelian randomization (MR) analysis was used to explore the causal relationship between drug targets and OA. In vivo, a triclocarban (TCC)-induced zebrafish OA model was treated with selected drugs, and transcriptomic sequencing, network pharmacology and molecular docking were performed to identify potential drug targets.

Results: We found OB populations as key OA-associated cells, differentially expressed genes in OBs were enriched in neutrophil (NE)-mediated immune pathways. Cell communication analysis revealed enhanced bidirectional OB-NE signaling in OA, primarily mediated through the CXCL12-CXCR4 and RETN-CAP1 pathways. Riluzole was identified as a therapeutic candidate through drug repositioning analysis. MR showed an inverse association between the expression of its target SLC7A11 and OA risk (OR=0.84, 95% CI=0.72–0.98, P=0.027). In zebrafish OA models, riluzole treatment significantly reduced joint degeneration and downregulated CTSS, NOS1 and key components of the MAPK/ERK pathway. Molecular docking studies demonstrated strong binding affinity of riluzole to CTSS and NOS1, suggesting that inhibition of these targets may underlie its therapeutic action via suppression of MAPK/ERK suppression.

Conclusion: This study highlights riluzole as a promising repositioned drug for OA. Limitations of this study include the relatively small sample size and the need for further translational validation in clinical settings.

Keywords: osteoarthritis, single-cell transcriptome sequencing, drug repositioning, riluzole, osteoblasts

Introduction

Osteoarthritis (OA) is a prevalent and multifactorial skeletal disorder characterized by progressive structural deterioration, including articular cartilage degradation, subchondral bone remodeling, osteophyte formation and synovial inflammation.[1] Despite its high prevalence and increasing burden, current OA treatments, which largely focus on symptom relief, often fail to address the underlying pathophysiology. The development of novel therapeutics remains

https://doi.org/10.2147/DDDT.S544803
Received: 17 June 2025
Accepted: 12 September 2025
Published: 11 April 2026

challenging due to the high cost, long timelines, and high attrition rates associated with traditional drug discovery pipelines. In this context, drug repurposing offers a promising strategy to identify novel therapeutic agents that may be more effective and safer for OA treatment.[2]

Osteoblasts (OBs), which mediate bone remodeling, chondrocytes, which maintain cartilage matrix metabolism, and synoviocytes, which regulate pro-inflammatory factors, play important roles in the development of OA. Currently, there are many studies on chondrocytes and synoviocytes, but few studies on osteoblasts in OA. OBs play a pivotal role in the pathogenesis of OA by depositing bone matrix proteins onto the calcified cartilage matrix, thereby initiating new bone formation in the subchondral region.[3–5] The close interplay between skeletal and immune systems -referred to as "osteoimmunology"- has been increasingly recognized, with dysregulated bone-immune cell interactions contributing to various skeletal diseases.[6,7] Single-cell RNA sequencing (scRNA-seq) enables high-resolution profiling of cell populations and their molecular signatures within complex tissues,[8] while cell-cell communication analysis facilitates the investigation of molecular interactions between distinct cell types.[9] Despite these advances, the specific intercellular communication patterns between OBs and immune cells, particularly in OA, remain largely unexplored.

Among immune cells, Neutrophils (NEs) contribute to joint pathology in OA by releasing pro-inflammatory factors, which disrupt bone and cartilage homeostasis.[10,11] Our prior work was among the first to apply freshly collected human femoral head samples, revealing cellular heterogeneity and identifying potential functional roles of various cell subsets in the OA microenvironment.[12] Another study have reported ligand-receptor interactions between immune cells and osteoblastic lineage cells, suggesting complex communication networks within the bone niche,[6] but the specific molecular mechanisms of OB-NE interaction in OA remain unclear.

Drug repositioning refers to identifying new therapeutic indications for existing approved drugs. Drug repositioning offers several advantages over de novo drug development, including reduced costs, shortened timelines, and improved clinical translation due to pre-established safety profiles.[13] For example, the Food and Drug Administration (FDA) approved drug memantine, originally indicated for Alzheimer's disease, has shown potential to delay cartilage degeneration and reduce OA-related pain.[14] Riluzole is an FDA-approved glutamate release inhibitor used to treat amyotrophic lateral sclerosis (ALS). Riluzole has been found to exert antitumor effects through drug repositioning studies.[15] However, few studies have utilized scRNA-seq data for drug repositioning in OA, and to date, none have focused on repositioning drugs targeting OB-NE interactions.

In our study, we conducted an integrative analysis of scRNA-seq datasets across multiple human femoral head samples to investigate the interaction between OBs and NEs in OA. Then we adopted a network-based drug repositioning approach, integrating scRNA-seq data with drug-target and protein-protein interaction networks to identify promising OA therapeutic candidates. To our knowledge, this is the first study to reposition drugs targeting OB and NE in OA. We further applied Mendelian randomization (MR) analysis to investigate causal relationship between drug targets and OA. Experimental validation in a zebrafish OA model, combined with transcriptomic profiling, network pharmacology, and molecular docking, allowed us to predict novel targets and elucidate the potential mechanisms of action of candidate compounds. Our findings provide a comprehensive framework for precision drug repurposing in OA and provide new insights into drug-mediated mechanisms.

Method

Study Samples

This study included three femoral neck fracture samples (control group) and three osteoarthritis patients (OA group). Femoral head tissues were obtained from patients undergoing hip replacement surgery at Xiangya Hospital, Central South University. Detailed sample information is provided in Table 1 and the diagnostic criteria refer to previously published article.[16] After surgery, the discarded samples were promptly collected, carefully packaged in sterile bags, and transported in an ice box to maintain appropriate temperature conditions. The samples were then rapidly transported to the laboratory for further processing. This research was approved by the Ethics Committee of Xiangya Hospital, Central South University (No. 201912315)., and conducted in accordance with the Declaration of Helsinki.

Table 1 The Sample Information Used in scRNA-Seq Analysis

ID	Age (Years)	Gender	Group
Control1	60	Male	Control
Control 2	62	Female	Control
Control 3	85	Female	Control
OA1	61	Female	OA
OA2	45	Female	OA
OA3	31	Male	OA

Cell Isolation and scRNA-Seq

In this study, Magnetic-Activated Cell Sorting (MACS) was utilized to isolate specific cells from femoral head samples. Briefly, after collection, the femoral head specimens were processed into small bone fragments and enzymatically digested using a tissue dissociation solution. The erythrocyte lysis buffer (Solarbio Science & Technology Co., Ltd, Beijing, China) was used to remove red blood cells. And the cells with low cell viability were removed by using a dead cell removal kit (Mitenyi Biotec, Germany). $CD45^{-}ALPL^{+}$ osteoblasts were enriched using magnetic bead-based sorting to ensure high specificity.

Single-cell transcriptome sequencing was then performed using the 10x Genomics platform (Chromium™ Controller, USA). Library preparation followed the manufacturer's guidelines outlined in the Single Cell 3′ Library & Gel Bead Kit V3 user manual (10x Genomics User Guide). Sequencing was performed to a minimum depth of 50,000 reads per cell with 150-bp paired-end reads. The resulting sequencing data were used for downstream bioinformatics analysis.

Data Preprocessing and Integration

Single-cell expression matrix files were imported using the Read10X function in the Seurat V5 package in R.[17] A Seurat object was then created using the CreateSeuratObject function for subsequent analysis and visualization. To ensure data quality, cells were excluded if they met any of the following criteria: gene count <200 or >8000, or mitochondrial and ribosome gene expression exceeded 5%. This stringent filtering strategy ensured the inclusion of only high-quality single-cell.

For dataset integration, we used the Find Integration Anchors function with the parameter dims = 1:20. To correct for potential batch effects across samples, we using the RunHarmony function.[18] Cell clustering was performed using the Find Clusters function with a resolution 0.6. Cell type annotation was conducted by cross-referencing known marker genes from the literature and using the CellMarker database[19] (http://bio-bigdata.hrbmu.edu.cn/CellMarker/search.jsp). For dimensionality reduction and visualization, the Uniform Manifold Approximation and Projection (UMAP) method was employed to distinguish and display different cell populations.

Identifying Disease-Associated Cells

To identify genome-wide association studies (GWAS)-associated cell types, we utilized the single-cell disease relevance score (scDRS) approach to establish connections between specific cell types and OA.[20] First, we employed the MAGMA[21] tool to generate disease-associated gene sets based on GWAS data for OA. Subsequently, we applied the scDRS to assess the relevance of each cell by quantifying the expression of putative disease-related genes across the entire cell population and calculating the disease association *p*-value at the single-cell level. The GWAS datasets for OA (ebi-a-GCST005812) analyzed in this study were obtained from the openGWAS database (https://gwas.mrcieu.ac.uk).

Differential Gene Expression Analysis

The subset function was used to extract OBs or NEs, and differential expression genes (DEGs) analysis was performed on OBs or NEs between the control and OA group using the Find Markers function. The criteria for identifying significant DEGs were $|avg\_log2FC| > 1.5$ and $p\_val\_adj < 0.05$.

https://doi.org/10.2147/DDDT.S544803

Functional Enrichment Analysis

To identify the significantly enriched pathways of DEGs or key genes, we employed the clusterProfiler package in R to perform GO enrichment analysis. Only terms with p_val_adj < 0.05 were considered as significantly enriched. Gene set enrichment analysis (GSEA) was performed by the R package "ClusterProfiler" with normalized corrected ES values > 1 and p-val_adj < 0.05 for significance.

Cell Communication Analysis

Intercellular communication was analyzed using the CellChat package in R.[9] Using CellChat, we identified distinct ligand and receptor expression patterns across various cell types. These analyses allowed us to identify unique signaling mechanisms for each cell population and uncover functional communication among different cell types.

Drug Repositioning Analysis

We employed a network-based approach for drug repositioning analysis.[2,22,23] Initially, known drug targets were mapped to the human proteome, which was subsequently mapped to disease modules. In this study, DEGs in OB and NE were first extracted from control and OA groups. These DEGs were then utilized to extract relevant interactions from the human interactome to construct the protein-protein interaction (PPI) network representing the disease modules. A drug-target network was built using drug-target interactions obtained from the DrugBank (https://go.drugbank.com/) and Therapeutic Target Database (TTD). After constructing the drug-target network, we calculated the network closeness between drug targets and disease modules. A higher network proximity, indicated by a lower Z-score, suggests stronger network relationships.

MR Analysis

To evaluate the causal association of drug targets with OA, we conducted MR analysis using the inverse-variance weighted (IVW) approach. Expression quantitative trait locis (eQTLs) from openGWAS database were used as instrumental variables. Single nucleotide polymorphisms (SNPs) that were strongly associated with the SLC7A11, PDE4A and VDR were selected based on a GWAS *p*-value threshold of 5×10^{-8}, along with a linkage disequilibrium (LD) $r^2 < 0.1$. The OA GWAS data (ebi-a-GCST005814) from openGWAS database was used as the outcome. Heterogeneity was assessed using Cochran's Q test, and pleiotropy was evaluated via MR-Egger intercept. Additionally, a leave-one-out analysis was conducted to systematically exclude individual SNPs and evaluate the influence of each SNP on the overall MR analysis results. Detailed information regarding the instrumental variables used in the analyses was provided in Tables S1–S3.

OA Zebrafish Model

Wild-type zebrafish were obtained from the Department of Genetics and Developmental Biology at Hunan Normal University. All animal experiments were approved by the Institutional Animal Care and Use Committee of Hunan Normal University. Based on previously published studies, zebrafish were exposed to 2μM Triclocarban (TCC, Solarbio, BeiJing, China) for 21 consecutive days. Successful model establishment was confirmed by histological staining, which revealed a marked narrowing of the anal fin joint space.[24] Adult zebrafish were randomly divided into 5 groups: a control group treated with 0.25% dimethyl sulfoxide (DMSO, Coolaber, BeiJing, China) and an OA model group treated with 2μM TCC. For the TCC-induced groups, 10 μg/mL chondroitin sulfate was administered in combination with TCC induction as the positive control group (TCC+Cho). Based on the clinical oral dose of riluzole (MCE, ShangHai, China) in human (50 mg/day), the equivalent dose for zebrafish was calculated to be approximately 10μM using body surface area conversion factors. However, our preliminary experiments revealed significant lethality at concentrations of 2.5, 5 and 10μM, while zebrafish exposed to 1 and 1.5 μM exhibited normal physiological activities. Therefore, we selected the concentration range of 1 and 1.5 μM for subsequent experimental investigations. The drug treatment groups received TCC induction combined with either 1 μM or 1.5 μM riluzole, designated as TCC+Ril (1) and TCC+Ril (1.5), respectively. After 21 days, zebrafishes were stained using Alcian blue and Alizarin red. The joint space at the anal fin of zebrafish was

quantified using Image J software to assess the success of OA modeling. Specifically, all measurements were conducted using a single-blind design, with the operator unaware of the group assignments to avoid subjective bias. For each zebrafish, the joint space of the same specific region of the anal fin was measured three times, and the final joint space value was calculated as the mean of the three repeated measurements to minimize random errors.

Bulk RNA-Seq and Data Analysis

Total RNA was extracted from the anal fin tissues of zebrafish in both the TCC group and TCC+Ril (1.5 μM) group. RNA quality was verified by agarose gel electrophoresis, and sequencing was performed using the BGI platform. RNA integrity, assessed with an Agilent 2100 Bioanalyzer, showed a RNA Integrity Number (RIN) > 8.0.

Strand-specific cDNA libraries were constructed through poly(A) selection and subsequently sequenced to generate 150-bp paired-end reads. The obtained reads were aligned to the zebrafish GRCz11 reference genome using the STAR aligner, achieving a mapping rate of over 90% for all samples.

Significant DEGs were identified using standard RNA-seq data analysis pipelines, with criteria set at $|avg\_log2FC| > 0.585$ and $p\_val\_adj < 0.05$. These DEGs were subsequently subjected to GO enrichment analysis.

Drug Target Prediction

The SMILES notation for riluzole was retrieved from the PubChem database (https://pubchem.ncbi.nlm.nih.gov/) and subsequently imported into the SwissTargetPrediction platform (http://www.swisstargetprediction.ch) to predict its potential drug targets. We then analyzed the intersection between these predicted targets and DEGs identified from transcriptome sequencing data to determine the final candidate targets of riluzole.

Molecular Docking

Molecular docking, a computational biology method, was employed to investigate the interactions between riluzole and its protein targets. The 2D structure of riluzole was obtained from PubChem (https://pubchem.ncbi.nlm.nih.gov/), while the 3D structures of the target proteins were downloaded from the Protein Data Bank (PDB; http://www1.rcsb.org/). Docking simulations were performed using AutoDock Vina, an open-source software, to evaluate binding affinities and conformational stability between riluzole and the targets.

Results

scRNA-Seq Combined GWAS Analysis Reveals Cells Associated with OA

We identified 26 clusters (Figure 1A) which were annotated into 10 cell types, 57772 cells in total: OB (23.51%), NE (56.70%), Chondrocytes (CHON, 1.01%), Erythrocytes (ER, 4.67%), Macrophages (MAC, 2.44%), B cells (B, 1.91%), T cells (T, 5.43%), plasma cells (PC, 1.72%), Endothelial cells (EC, 1.34%), Smooth muscle cells (SMC, 1.27%), based on previously reported marker genes and cell marker genes provided by the CellMarker database (Figure 1B), a summary table in Table 2. To identify cells associated with OA, we utilized scDRS analysis to integrate scRNA-seq data with GWAS data. UMAP plots demonstrated that cells associated with OA (Figure 1C) was predominantly enriched in OB cell cluster. This finding suggests that OBs play a central role in the pathogenesis of OA, and highlights their potential as a key focus for further investigation in our study.

To investigate the functions of genes in OB, we performed differential expression analysis. The volcano plot in Figure 1D illustrates genes that exhibit significant differences between control and OA groups. GO enrichment analysis revealed that the DEGs in OB of OA were significantly enriched in pathways related to oxidative stress, inflammation and immune-related pathways, especially NE-mediated immune signaling pathways (Figure 1E). The enrichment in NE-mediated immune signaling pathways suggests that differential genes of OBs in the OA group are associated with the function of NE.

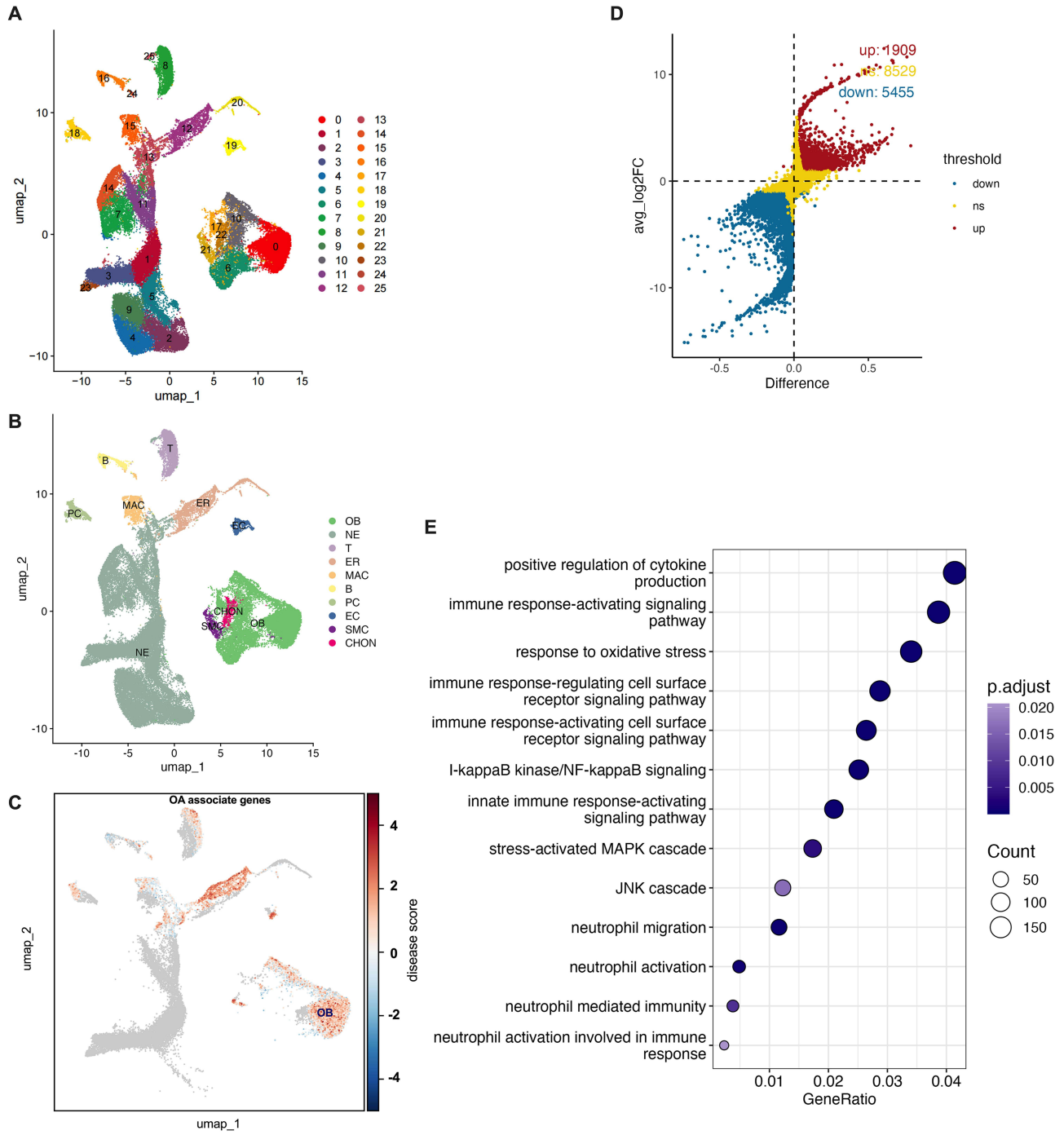

Figure 1 Cell type annotation and identification of OA-associated cell populations. (**A**) Clustering analysis at a resolution of 0.6 identified 26 clusters in the integrated dataset, with distinct colors representing each cluster. (**B**) Based on marker gene distribution, a total of 10 cell types were annotated. (**C**) Distribution of OA related cells across various cell types. Cells significantly correlated with disease are highlighted in red, where higher correlation values indicate stronger associations. (**D**) Differential expression analysis of genes was performed in OB between the OA and control groups. Red dots represent genes highly expressed in the OA group, while blue dots indicate lower expression. (**E**) GO enrichment analysis of DEGs.

Cellular Communication Between Different Cell Types Across Groups

To investigate the intercellular communication, we analyzed the intercellular communication network using the CellChat package. Comparative analysis of interaction strength revealed significantly enhanced interactions from NE to OB and from OB to NE in the OA group (Figure 2A). CellChat analysis revealed ligand-receptor (L-R) interactions between OBs and other cells (Figure S1). Specifically, in the OA group, cellular communication from OB to NE was mediated by the

https://doi.org/10.2147/DDDT.S544803

Table 2 A Summary Table for Each Cell Type

Cell Type	Cell Count	Mean Reads	Median Genes	Total Reads	Detected Genes
OB	13580	7826.71	2409	106286723	28556
NE	32759	3215.96	795	105351560	26858
T	3136	5198.32	1650.5	16301929	19025
ER	2696	25752.5	1721	69428739	22626
MAC	1409	8972.82	2310	12642704	18444
B	1104	5108.52	1779.5	5639808	17689
PC	994	28108.36	2513	27939711	20131
EC	773	11734.78	2695	9070982	22977
SMC	736	8395.93	2538	6179404	23392
CHON	585	19397.25	3883	11347394	24447
TOTAL	57772	6407.757287	1419	370188954	29864

CXCL12-CXCR4 (CXCL pathway) L-R pair (Figure 2B), while communication from NE to OB was mediated through the RETN-CAP1 (RESISTIN pathway) L-R pair (Figure 2C). Notably, the RETN-CAP1 L-R pair was exclusively involved in NE-OB interactions and not in other cell-OB communications.

Key signaling pathways were ranked based on the differences in overall information flow inferred across the different groups. Both the CXCL and RESISTIN signaling pathways were significantly enriched in the OA group (Figure 2D). Previous studies have reported that RESISTIN upregulated the expression of inflammatory cytokines in human OA,[25] and the CXCL12/CXCR4 axis promoted cartilage degradation.[26] These findings suggest that the enhanced information flow of RESISTIN and CXCL in OA group may disrupt the bone microenvironment.

The circle diagram provides a more intuitive representation of changes in CXCL signaling during OB communication with other cells, revealing that CXCL signaling between OB and NE was stronger in OA (Figure 2F) compared to control group (Figure 2E). For RESISTIN pathway, the results showed that, unlike in the control group (Figure 2G), this pathway mediated cellular communication exclusively from NE to OB in OA group (Figure 2H).

Functional Analysis of the DEGs in NE

Cellular communication analysis revealed a significant increase in communication strength between OB and NE in OA. This finding suggests that NE may play a crucial role in the development of OA. Therefore, we further investigated the function of NE. Initially, differently expression analysis was conducted on NE from the OA group and the control group (Figure 3A). GO enrichment analysis revealed that the DEGs in the OA group were enriched in immune-related pathways such as “immune response-regulating signaling pathway” and “immune response-activating signaling pathway”, as well as in typical inflammatory pathways, including “I-kappaB kinase/NF-kappaB signaling”. Additionally, these DEGs were significantly enriched in bone metabolism-related signaling pathways, including “osteoclast development” and “bone cell development” (Figure 3B). These results indicate that the DEGs in NE are implicated in bone metabolism.

Drug Repositioning Analysis

Building on the results obtained, we conducted a drug repositioning analysis targeting OB and NE cells. Using screening criteria of $Z < -2$ and $P < 0.05$, and after excluding small-molecule compounds, metal-based drugs and radioactive ligands, we identified 34 candidate drugs in the OB group and 79 candidate drugs in the NE group, with 25 overlapping drugs between the two groups (Figure 4A; detailed information provided in Table 3). The targets of these 25 drugs were retrieved from DrugBank, and MR analysis was performed to evaluate causal relationships between these targets and OA (target list in Table 4). The IVW results revealed significant causal associations between the gene expression of drug targets SLC7A11 (OR=0.84, 95% CI=0.72–0.98, P= 0.027), PDE4A (OR=1.14, 95% CI=1.01–1.28, P=0.028) and VDR (OR=0.92, 95% CI=0.86–0.98, P=0.011) with OA (Figure 4B).

Cochran’s Q test and MR-Egger intercept analysis demonstrated no evidence of heterogeneity (Table 5) or horizontal pleiotropy (Table 6) in the MR analysis. To further assess whether the results were influenced by individual SNPs,

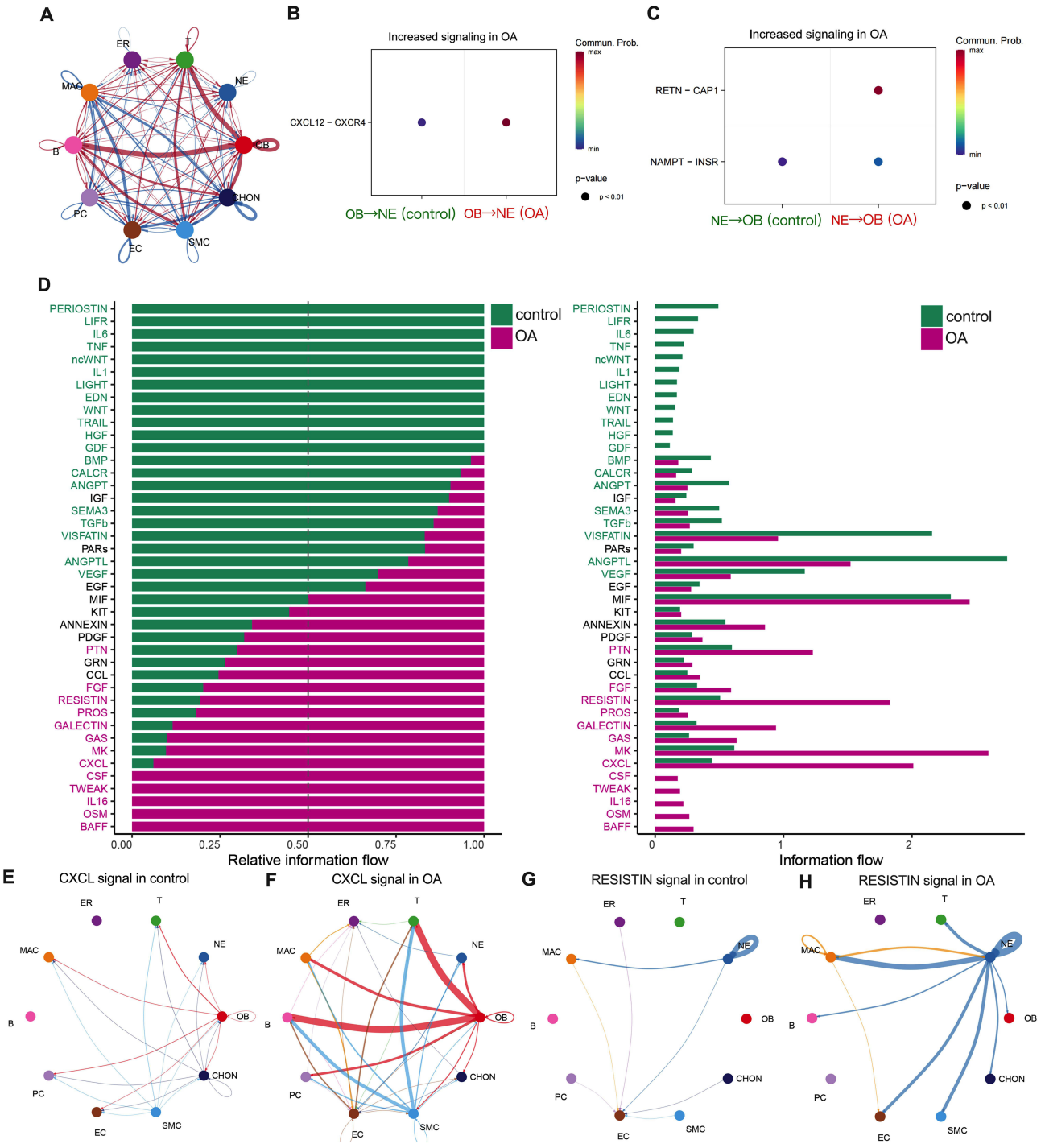

Figure 2 Cell communication analysis. (**A**) Compared to the control group, changes in cell communication strength between different cell types in the OA group. Red indicates enhanced communication, while blue indicates reduced communication. (**B** and **C**) Ligand-receptor pair mediating OB-to-NE (**B**) and NE-to-OB (**C**) communication. (**D**) Comparative analysis of information flow strength between the OA and control groups. (**E** and **F**) Visualization of CXCL signaling using a circle chart, with OB as the sender in control and OA group. (**G** and **H**) Visualization of RESISTIN signaling using a circle chart, with NE as the sender in control and OA group.

a leave-one-out sensitivity test was conducted (Figure 4C–E). The results indicated that the causal effect of SLC7A11, PDE4K and VDR on the OA did not significantly change upon excluding any single SNP. Detailed information for OA-related SNPs is provided in Tables S1-3.

Notably, the gene expression of riluzole target SLC7A11 and cholecalciferol target VDR exhibited significant reverse causal effects on OA, while riluzole and cholecalciferol act agonistic activity toward SLC7A11 and VDR, respectively.

https://doi.org/10.2147/DDDT.S544803

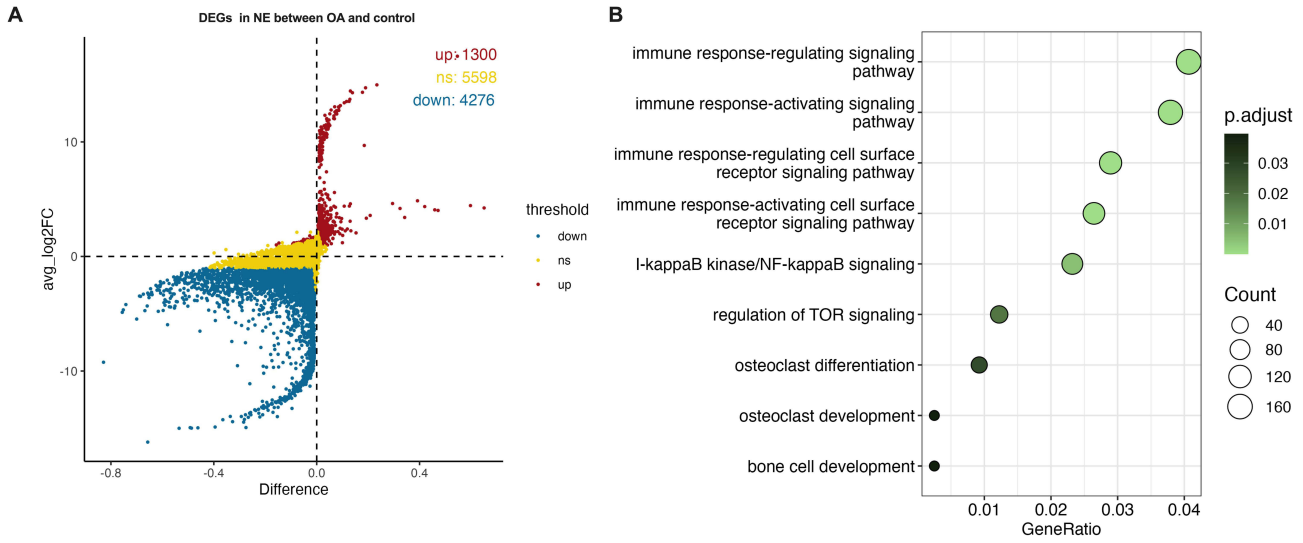

Figure 3 The GO enrichment analysis of DEGs in NE. (**A**) DEGs identified in NE between OA group and control group. (**B**) GO enrichment analysis of NE-specific DEGs.

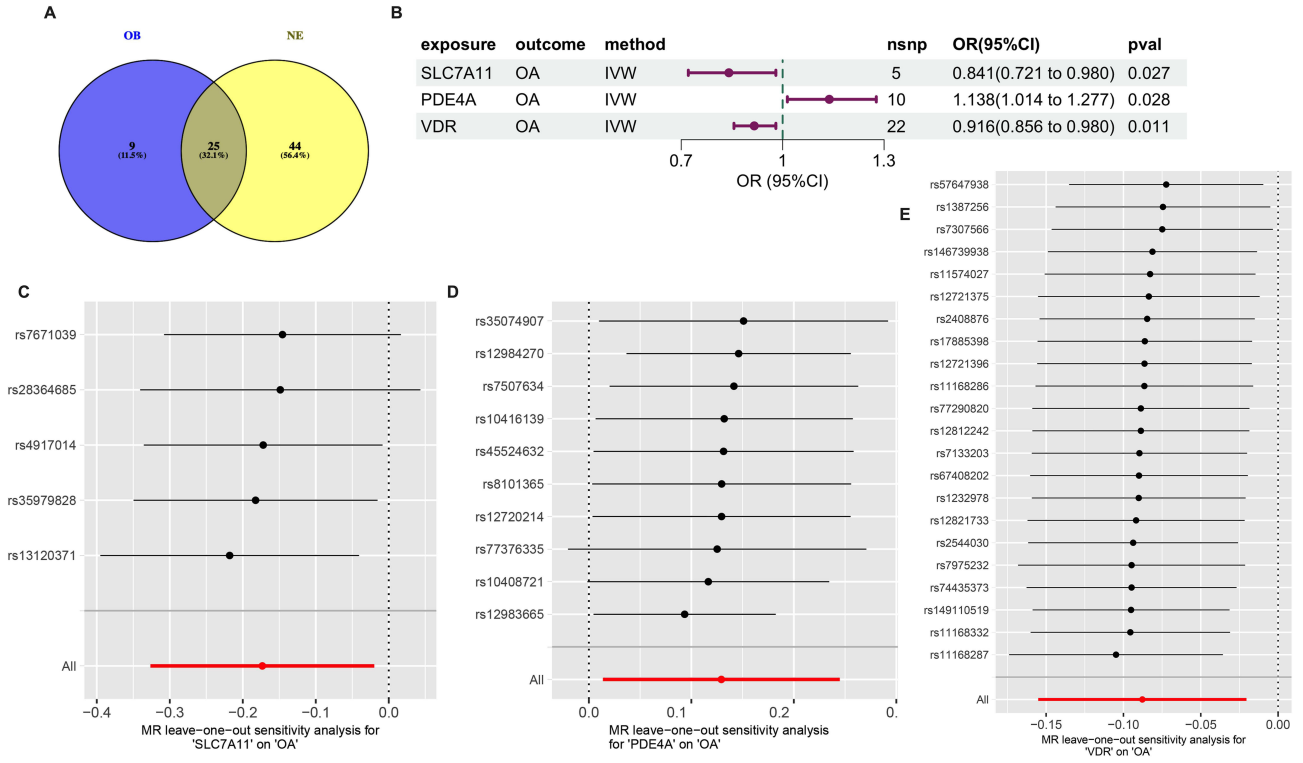

Figure 4 Drug repositioning and causal effects between the drug targets and OA. (**A**) The intersection of drugs simultaneously screened in OB and NE. (**B**) The drug targets SLC7A11, PDE4A, and VDR show significant causal relationships with OA. Leave-one-out analysis of the targets SLC7A11 (C), PDE4A (D), and VDR (**E**) in relation to OA.

These findings suggest their potential therapeutic efficacy against OA. Conversely, the expression of apremilast target PDE4A showed a significant positive causal effect on OA, while apremilast acts as a PDE4A antagonist, indicating its therapeutic potential role in OA management.

Cholecalciferol (vitamin D3) is known to inhibit synovial fluid effusion[27] and improve the Western Ontario and McMaster Universities Arthritis Index pain score after 12-month supplementation.[28] Apremilast has been shown to prevent chondrocyte senescence[29] and suppress inflammatory responses in chondrocytes by upregulating SOX9.[30]

https://doi.org/10.2147/DDDT.S544803

Table 3 Network Proximity Scores for Common Drugs for OB and NE

DrugBank ID	Drug Name	OB			NE		
		D-value	Z-value	P-value	D-value	Z-value	P-value
DB00091	Cyclosporine	2.142	−3.442	0	2.154	−3.298	0
DB00169	Cholecalciferol	2.158	−2.209	0	2.177	−2.051	0.001
DB00308	Ibutilide	2.191	−2.144	0.008	2.2	−2.016	0.008
DB00337	Pimecrolimus	2.137	−2.063	0.004	2.143	−2.316	0.005
DB00419	Miglustat	2.191	−2.097	0.002	2.196	−2.524	0.001
DB00456	Cefalotin	2.095	−2.039	0.007	2.098	−2.462	0.003
DB00640	Adenosine	2.088	−3.157	0	2.093	−3.203	0
DB00651	Dyphylline	2.181	−2.464	0	2.167	−3.178	0
DB00677	Isoflurophate	2.17	−2.416	0	2.173	−2.658	0.001
DB00730	Thiabendazole	2.117	−2.1	0.003	2.125	−2.228	0.004
DB00740	Riluzole	2.187	−2.493	0	2.183	−3.087	0
DB00746	Deferoxamine	1.918	−2.563	0.01	1.934	−2.494	0.016
DB00878	Chlorhexidine	2.073	−2.265	0.003	2.074	−2.613	0.002
DB00903	Etacrynic acid	2.088	−2.584	0	2.1	−2.242	0.003
DB01427	Amrinone	2.045	−2.739	0	2.044	−3.315	0
DB01590	Everolimus	2.145	−2.29	0.001	2.15	−2.825	0
DB03424	Ubenimex	2.182	−2.087	0	2.182	−2.492	0
DB05018	Migalastat	2.179	−2.058	0.002	2.19	−2.241	0.002
DB05219	Crisaborole	2.197	−2.3	0	2.186	−2.445	0
DB05676	Apremilast	2.127	−2.256	0.005	2.135	−2.272	0.001
DB06287	Temsirolimus	2.124	−2.782	0	2.127	−3.097	0
DB08168	Coumarin 120	2.111	−3.671	0	2.122	−3.432	0
DB09074	Olaparib	2.109	−2.348	0.002	2.111	−2.575	0
DB09283	Trapidil	2.126	−2.942	0	2.104	−4.521	0

Although riluzole has not been extensively studied in the context of OA, it was prioritized as a novel candidate for further analysis. These findings also demonstrate the feasibility of the method used for screening candidate drugs for OA.

Effects of Riluzole on OA in Zebrafish

To investigate whether riluzole alleviates TCC-induced OA symptoms in zebrafish, adult zebrafish were co-exposed to TCC and riluzole at different concentrations (1 μM and 1.5 μM) for 21 days. Alcian Blue-Alizarin Red double staining revealed changes in anal fin joint space following drug treatment (Figure 5A). Compared to control group, the TCC group exhibited a narrowed anal fin joint space, confirming successful modeling of OA. In contrast, the TCC+Ril (1 μM) and TCC+Ril (1.5 μM) groups showed significantly widened joint spaces (the distance between cartilage and hard bone), with the most pronounced effect in the TCC+Ril (1.5 μM) group (Figure 5B), indicating riluzole's inhibitory effect on OA progression.

To further explore riluzole's mechanism of action, anal fin tissues from the TCC and TCC+Ril (1.5 μM) groups were subjected to transcriptome sequencing. Differential gene expression analysis identified both upregulated and down-regulated genes (Figure 5C). GO enrichment analysis of DEGs revealed that riluzole treatment significantly DEGs enriched in inflammatory pathways, including "inflammatory response", "response to interleukin-1" and "response to tumor necrosis factor", as well as pathways such as positive regulation of MAPK/ERK signaling and "regulation of catalytic activity" (Figure 5D). The heatmap shows the expression of key genes in the MAPK/ERK signaling pathway in both groups (Figure 5E), and riluzole inhibited the mRNA expression levels of key genes in the MAPK/ERK signaling pathway (Figure 5F). The above results indicate that riluzole suppresses the inflammatory response, the MAPK/ERK signaling pathway and the catalytic activity of enzymes.

Table 4 Target Information for Each Drug

DrugBank ID	Drug Name	Target	Actions
DB00640	Adenosine	ADORA1	Activitor
DB01427	Amrinone	PDE3A	Inhibitor
DB05676	Apremilast	PDE4A	Inhibitor
DB00456	Cefalotin	pbpA	Inhibitor
DB00878	Chlorhexidine	Bacterial outer membrane	Incorporation into and destabilization
DB00169	Cholecalciferol	VDR	Activitor
DB08168	Coumarin 120	PPIA	Inhibitor
DB05219	Crisaborole	PDE4B	Inhibitor
DB00091	Cyclosporine	PPP3R2	Inhibitor
DB00746	Deferoxamine	APP	Unknown
DB00651	Dyphylline	PDE4B	Inhibitor
DB00903	Etacrynic acid	SLC12A1	Inhibitor
DB01590	Everolimus	MTOR	Inhibitor
DB00308	Ibutilide	KCNH2	Inhibitor
DB00677	Isoflurophate	ACHE	Inhibitor
DB05018	Migalastat	GLA	Stabilization
DB00419	Miglustat	UGCG	Inhibitor
DB09074	Olaparib	PARP1	Inhibitor
DB00337	Pimecrolimus	PPP3CA	Inhibitor
DB00740	Riluzole	SLC7A11	Activitor
DB06287	Temsirolimus	MTOR	Inhibitor
DB00730	Thiabendazole	FRDA	Inhibitor
DB09283	Trapidil	FGFR3	Inhibitor
DB03424	Ubenimex	LTA4H	Inhibitor

Table 5 The Results of Cochran's Q Test in the MR Analysis

Outcome	Exposure	Method	Q	Q_df	Q_pval
OA	VDR	MR Egger	25.216	20	0.193
OA	VDR	IVW	26.621	21	0.184
OA	SLC7A11	MR Egger	1.828	3	0.609
OA	SLC7A11	IVW	1.832	4	0.766
OA	PDE4A	MR Egger	15.191	8	0.055
OA	PDE4A	IVW	16.245	9	0.062

Abbreviation: IVW, inverse-variance weighted.

Table 6 The Results of MR-Egger Intercept Analysis in the MR Analysis

Outcome	Exposure	Egger_Intercept	se	pval
OA	VDR	0.0156	0.015	0.304
OA	SLC7A11	0.0016	0.021	0.956
OA	PDE4A	0.0126	0.016	0.477

Molecular Docking

In our previous analysis, we examined the causal relationship between riluzole's known targets and OA, however, potential reported targets of riluzole warrant further explored. We identified 89 potential targets of riluzole from the SwissTargetPrediction database (Table S4), of which 5 targets were significantly DEGs in the TCC+riluzole group (Figure 6A). Table S5 displays the top 40 differentially expressed genes. These five genes include ctss2 (orthologous to human CTSS; cathepsin S), nos1

https://doi.org/10.2147/DDDT.S544803

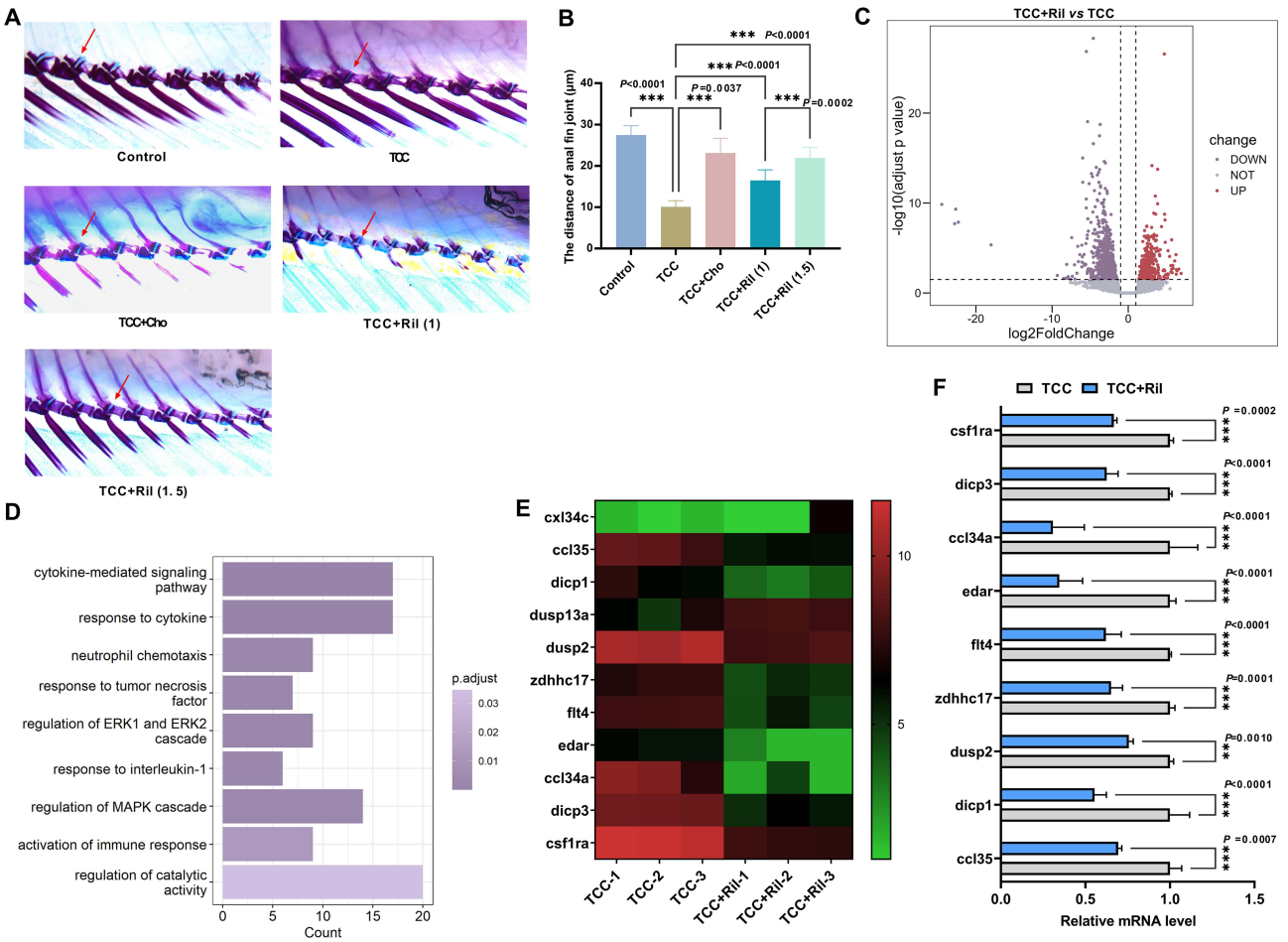

Figure 5 In Vivo Validation of Riluzole Efficacy and Transcriptome Sequencing. (**A**) Alcian blue-Alizarin red double staining was performed on a TCC-induced zebrafish osteoarthritis model after 21 days of drug treatment. The red arrow indicates the joint space. (**B**) Quantification of the joint space in the anal fins of zebrafish across groups. (**C**) Transcriptome sequencing was conducted on anal fin tissues of zebrafish, followed by analysis of DEGs between the TCC+Ril (1.5) group and the TCC group. (**D**) Bar plot showing the signaling pathways enriched by the DEGs mediated by riluzole. (**E**) The heatmap shows the expression of key genes in the MAPK/ERK signaling pathway in both groups. (**F**) The mRNA expression level of key genes in the MAPK/ERK signaling pathway in two groups. (*** P <0.001).

(orthologous to human NOS1; nitric oxide synthase 1), qpct (orthologous to human QPCT; glutaminyl-peptide cyclotransferase), pi4kaa (orthologous to human PI4KA; phosphatidylinositol 4-kinase alpha), plcg2 (orthologous to human PLCG2; phospholipase C gamma 2). All five genes were significantly downregulated in the TCC+riluzole group, with detailed information provided in Table 7. Figure 6B shows the 2D and 3D molecular structures of riluzole.

We utilized AutoDock software to analyze potential interactions between riluzole and these candidate proteins. The scoring function in AutoDock indicates that stable binding between ligand and protein molecules occurs when the docking affinity value is less than 0, with a more negative binding score reflecting stronger binding stability. The results demonstrate strong binding capabilities of riluzole with CTSS, NOS1, PLCG2, QPCT and PI4KA (Table 8). Among them, CTSS and NOS1 showed the strongest binding energy with riluzole at −7 kcal/mol and −6.9 kcal/mol, respectively.

Figure 6C and D illustrate the binding interactions of riluzole with the targets CTSS and NOS1, respectively. The molecular docking analysis revealed that riluzole effectively binds to the active pockets of these targets. Hydrogen bonds were formed between riluzole and amino acid residues GLN (Glutamine)-316, HIS (Histidine)-287 and ASP (Aspartic acid)-315 of CTSS (Figure 6C). Additionally, hydrogen bonds are observed between riluzole and the residues HIS-719 and GLN-530 of NOS1 (Figure 6D). The binding interactions of riluzole with PLCG2, QPCT and PI4KA are detailed in Figure S2A–C. The residues TYR (Tyrosine)-1884 and LEU (Leucine)-1862 of PI4KA establish hydrogen bonds with riluzole (Figure S2A). Additionally, riluzole forms a hydrogen bond with the amino acid residue PHE (Phenylalanine)-295 of PLCG2 (Figure S2B). Hydrogen bonds are also observed between riluzole and the residues GLU-202 and ASP-159 of QPCT (Figure S2C).

 https://doi.org/10.2147/DDDT.S544803

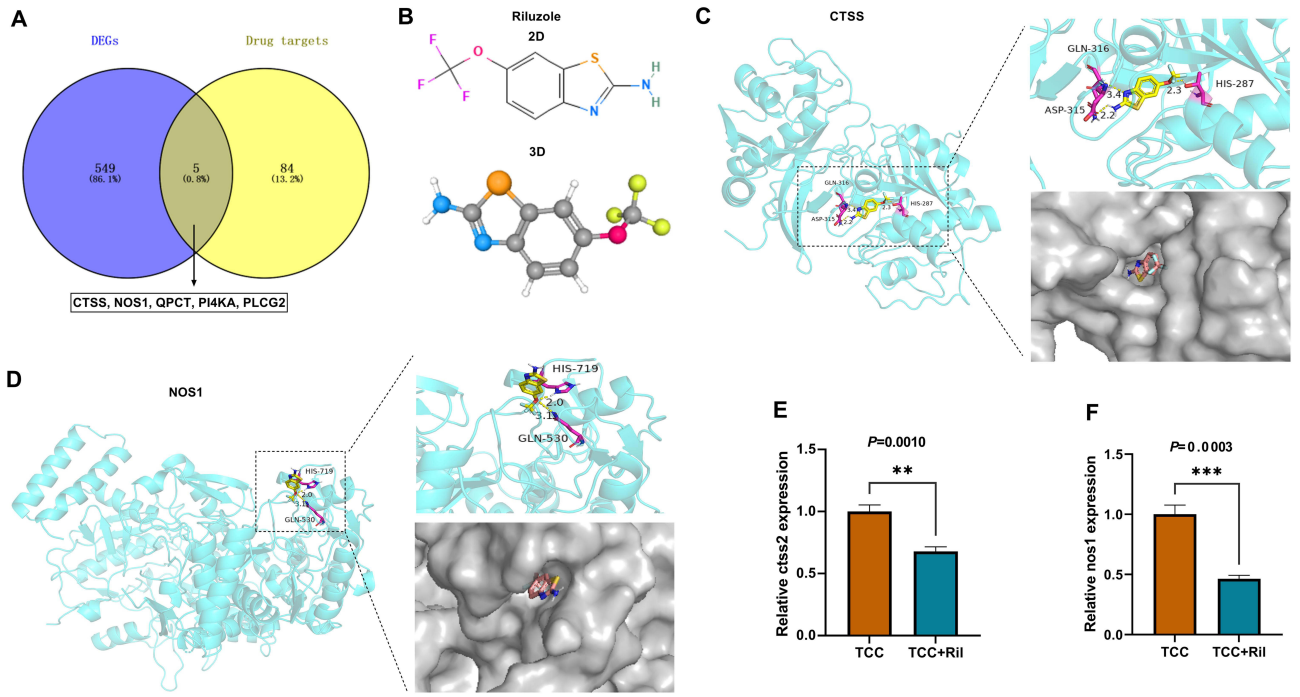

Figure 6 Result of molecular docking. (**A**) Intersecting genes between the potential targets of riluzole predicted by the SwissTargetPrediction database and DEGs after riluzole treatment. (**B**) 2D and 3D molecular structures of riluzole. Molecular docking results of riluzole with the potential targets CTSS (**C**) and NOS1 (D), which are involved in catalytic activity-related signaling pathways. Significantly downregulated expression of ctss2 (**E**) and nos1 (**F**) after riluzole treatment. (** P <0.01, *** P <0.001).

Furthermore, riluzole treatment significantly suppressed ctss2 (Figure 6E), nos1 (Figure 6F), pi4kaa (Figure S2D), plcg2 (Figure S2E) and qpct (Figure S2F) expression in a TCC-induced zebrafish OA model. Taken together, these findings provide strong evidence that riluzole slows OA progression by downregulating the expression of CTSS and NOS1.

Table 7 Differential Expression Analysis of Drug Targets in the TCC+Ril Vs TCC Group

Gene	log2 Fold Change	*p*_value	*p*_adj Value
ctss2	−3.377	1.62E-04	3.93E-03
nos1	−3.385	4.81E-05	1.46E-03
qpct	−4.580	1.48E-05	5.50E-04
pi4kaa	−2.132	1.23E-05	4.74E-04
plcg2	−2.178	9.05E-10	1.51E-07

Notes: ctss2, orthologous to human CTSS (cathepsin S). nos1, orthologous to human NOS1 (nitric oxide synthase 1). qpct, orthologous to human QPCT (glutaminyl-peptide cyclotransferase). pi4kaa, orthologous to human PI4KA (phosphatidylinositol 4-kinase alpha). plcg2, orthologous to human PLCG2 (phospholipase C gamma 2).

Table 8 Analysis of Docking Results Between Compounds and Targets

Compound	Target	PDB ID	Binding Energy (kcal/mol)
riluzole	CTSS	4MZS	−7
	NOS1	6PNG	−6.9
	PLCG2	8T7C	−6.9
	QPCT	2AFW	−6.6
	PI4KA	6BQ1	−6.3

https://doi.org/10.2147/DDDT.S544803

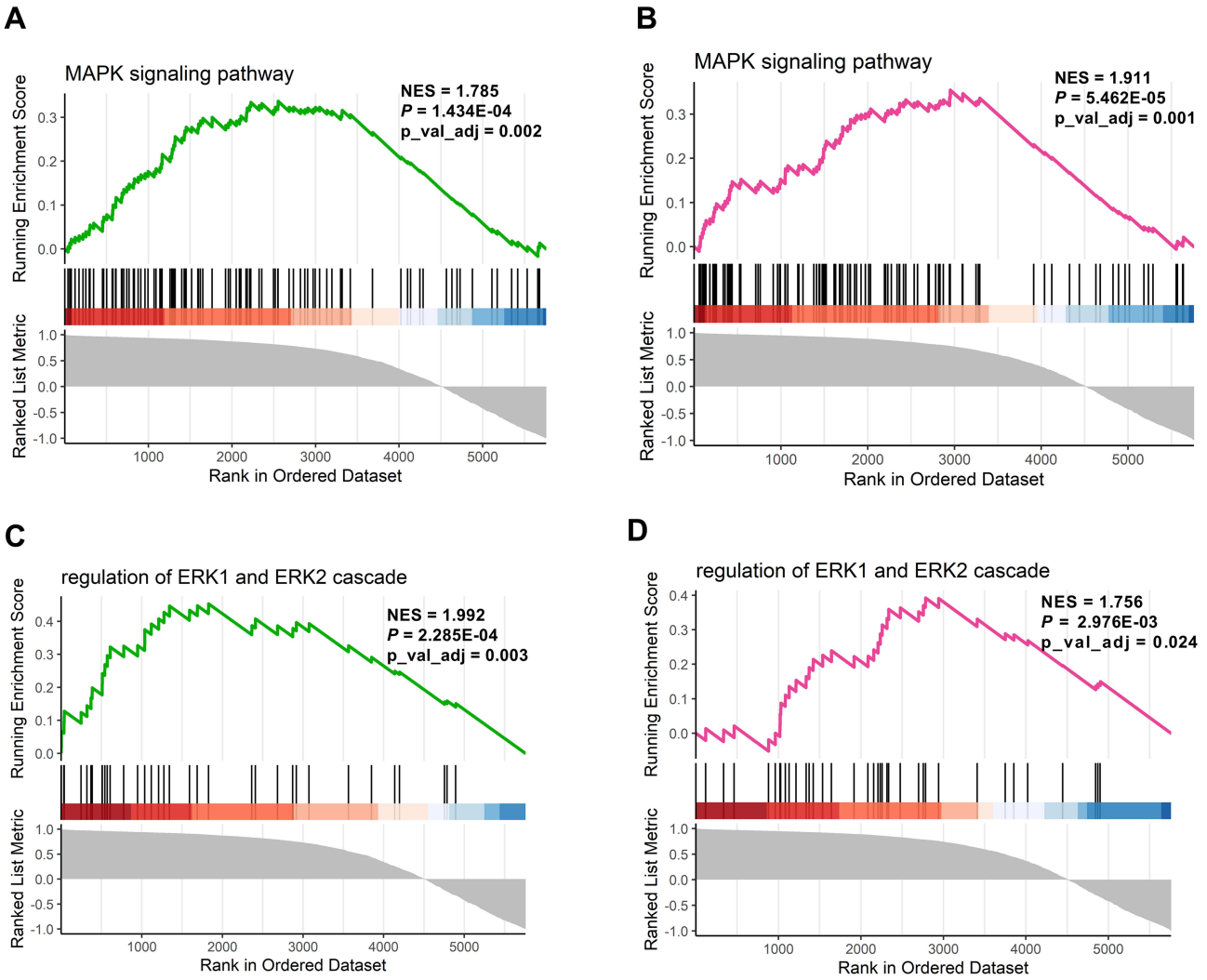

Figure 7 Result of GSEA. GSEA revealing the significant positive association between ctss2 expression and MAPK signaling pathway (**A**), nos1 expression and MAPK signaling pathway (**B**), ctss2 expression and ERK signaling pathway (**C**), nos1 expression and ERK signaling pathway (**D**).

CTSS and NOS1 Regulate MAPK/ERK Pathway

To further investigate the regulatory mechanism of riluzole's targets CTSS and NOS1, we performed GSEA analysis of CTSS and NOS1, and found that ctss2 (Figure 7A) and nos1 (Figure 7B) activate the MAPK pathway. Meanwhile, ctss2 (Figure 7C) and nos1 (Figure 7D) also activate the ERK pathway. Given that riluzole inhibits the expression of ctss2 and nos1 in zebrafish, along with the downregulation of genes in the MAPK/ERK pathway, we can infer that riluzole, as a drug with inhibitory effects on OA by inhibiting the activation of MAPK/ERK by target CTSS and NOS1.

Discussion

OA is a common multifactorial degenerative joint disease. ScRNA-seq technology enables precise identification of cellular constituents within highly heterogeneous lesioned tissues. By comparing control tissues, this approach facilitates a systematic investigation into functional alterations across distinct cell populations and changes in intercellular communication networks within pathological microenvironments, ultimately providing mechanistic insights for targeted therapeutic development.

Building upon this foundation, we integrated scRNA-seq data derived from femoral head tissues to identify OA-associated cell types through scDRS analysis. Cell communication analysis revealed significantly altered communication intensities between specific cell populations in OA group. Then, functional enrichment analysis and drug repositioning

analysis were performed on the DEGs of these cell types between OA and control groups. After screening candidate compounds, we administered the selected drugs to OA zebrafish models, monitored phenotypic changes and performed transcriptome sequencing. Subsequent network pharmacology analysis identified novel drug targets, which provides a new therapeutic candidate for the treatment of OA.

While some studies have utilized scRNA-seq to explore murine OBs,[31] but there have been limited research on human primary OBs isolated from hard bone tissue. This limitation was due to the specific mechanical hardness of hard bone tissue, which presented challenges in sample processing, and the relatively low abundance of OBs, making it difficult to isolate individual cells. Additionally, stably obtaining a single-cell suspension enriched with OBs is extremely challenging.[12,32] In this study, through extensive pre-experiment exploration, we developed a relatively robust cell dissociation protocol for enriching OBs by adjusting digestion conditions and using the MASC method. We utilized scRNA-seq to analyze freshly isolated primary cells from the femoral head, allowing for a more comprehensive understanding of the transcriptional characteristics of local cells.

Using the scDRS method to integrate single-cell data and GWAS data, we found that OA-associated cells were predominantly localized within OB populations. Compared to the control group, the DEGs in the OA group of OB were significantly enriched in pathways associated with oxidative stress, I-kappaB kinase/NF-kappaB signaling, MAPK signaling, JNK signaling and NE-mediated immunity. The activation of MAPK,[33] JNK[34] and Nf-κB[34] signaling pathways has been shown to drive inflammatory responses.[35] NE also emerged as a pivotal player in maintaining bone homeostasis. Hyperactivation of NEs could induce OB apoptosis by increasing ROS levels and promoting osteoclastogenesis via RANKL signaling.[36] Notably, in rheumatoid arthritis, activated NEs induces RANKL expression, enhancing osteoclast-mediated bone resorption in inflamed joints.[37] These findings suggest that the DEGs identified in OB are integrally involved in NE-mediated immune responses, highlighting their potential role in the complex interplay between inflammation, oxidative stress, and bone remodeling.

Interactions among diverse cell types within the bone microenvironment are essential for maintaining bone homeostasis.[6,7] The analysis revealed enhanced cellular communication between OB and NE, the RESISTIN and CXCL signaling pathways are significantly up-regulated in the OA group compared to the control group. In OA, RESISTIN promoted the secretion of pro-inflammatory factors such as TNF-α and IL-1β, with high expression of RESISTIN positively correlated with disease severity.[25] Similarly, the CXCL signaling pathway has been implicated in promoting inflammation and cartilage degradation, thereby contributing to the progression of OA.[26] We propose that this enhanced cellular communication between OB and NE may activate key signaling pathways, including RESISTIN and CXCL, which are involved in inflammation and tissue remodeling, and may contribute to the progression of OA. Osteoblast-derived signals like CXCL chemokines may further recruit and activate NEs, creating a feed-forward inflammatory loop that promotes subchondral bone sclerosis. Elevated levels of RESISTIN and CXCL family members may induce MMP expression in chondrocytes and accelerate extracellular matrix degradation and amplify synovial inflammation, indirectly contributing to pain, swelling, and joint dysfunction in OA patients.

Functional enrichment analysis of DEGs in NE cells revealed that these DEGs are not only implicated in immune-related signaling pathways but also regulate osteogenesis-associated pathways, such as "osteoblast differentiation" and "bone cell development". This finding further supports the theoretical premise that cellular communication between OB and NE is enhanced under OA disease conditions, also provides a theoretical foundation for subsequent drug repurposing analyses targeting NE and OB cells.

Current clinical therapies for OA patients fail to modify disease progression. Recent advances in network medicine have enabled the systematic repurposing of existing drugs.[2] In this study, we implemented an innovative network proximity-based drug repositioning strategy, constructing disease-specific network modules for OA by integrating single-cell sequencing data. By conducting in-depth analysis of the network proximity between the OA disease module and drug-target modules, combined with MR analysis to validate causal relationships between candidate drug targets and OA, we selected candidate drugs riluzole, cholecalciferol and apremilast. All three compounds exhibit anti-OA potential: cholecalciferol reduces synovial effusion[27] and pain;[28] Apremilast mitigates chondrocyte aging[29] and inflammation;[30] While riluzole emerges as a novel candidate requiring further exploration in OA therapeutics.

Riluzole, a glutamate release inhibitor, is a neuroprotective agent approved for the treatment of amyotrophic lateral sclerosis, a neurodegenerative disorder. In damaged joint, the release of glutamate promotes pain and induces inflammation and degeneration.[38,39] Memantine, also FDA-approved drug for the treatment of Alzheimer's disease, exerts its therapeutic effects by blocking the function of its downstream N-methyl-D-aspartate receptor (a subtype of glutamate receptor) in the central nervous system. In a drug repositioning study for OA, memantine was found to not only prevents cartilage degeneration but also aid in pain management.[14] This evidence highlights the potential of repurposing glutamate inhibitors, for the treatment of OA. In this study, the concentration of riluzole used in zebrafish (1–1.5 μM) is significantly lower than the therapeutic dose for human ALS. It is hypothesized that a lower dose may be needed for OA treatment, which may reduce the risk of elevated liver enzymes and central nervous system (CNS) side effects. While riluzole has an established safety profile in ALS treatment, its long-term use in OA patients warrants careful consideration, particularly regarding liver function and CNS side effects. These concerns should be addressed in future clinical trials, including dose-response studies specific to OA.

To further validate the therapeutic effects of riluzole, we established an OA zebrafish model and administered riluzole. Phenotypic observations revealed that riluzole treatment increased the joint space in the anal fin, indicating a protective role in articular cartilage. Subsequent transcriptomic sequencing analysis of drug-treated zebrafish demonstrated that riluzole administration significantly suppressed inflammatory pathways, MAPK signaling pathways, and catalytic activity-associated signaling pathways.

Although riluzole has known therapeutic targets, the discovery of novel targets could expand its therapeutic indications and enhance its clinical value. In this study, we employed online platforms to predict potential targets of riluzole and identified overlapping targets by intersecting these predictions with DEGs from riluzole-treated samples. Molecular docking analysis revealed that CTSS and NOS1 are potential novel targets of riluzole. CTSS, a lysosomal cysteine protease, effectively hydrolyze aggrecan after release at the site of inflammation, leading to the destruction of the chondrocyte extracellular matrix.[40] NOS1 is a key enzyme that catalyzes the production of NO, excessive NO could accelerate cartilage degradation in OA by promoting chondrocyte apoptosis and inhibiting cartilage repair mechanisms.[41] Additionally, NO derived from NOS1 may exacerbate joint damage by promoting oxidative stress, thus driving further disease progression.[42] Among the five potential targets (CTSS, NOS1, PLCG2, QPCT, and PI4KA), CTSS and NOS1 were prioritized because (i) both demonstrated the strongest binding affinities in docking analysis, and (ii) previous studies have reported significant associations of CTSS and NOS1 with OA pathogenesis. By contrast, the roles of PLCG2, QPCT, and PI4KA in OA remain poorly characterized, and no direct evidence has yet linked them to OA progression. Therefore, CTSS and NOS1 were highlighted as the most biologically relevant and mechanistically plausible targets for riluzole in the current study.

To further investigate the mechanism of CTSS and NOS1, we performed GSEA analysis of single genes and showed that CTSS and NOS1 activate the MAPK/ERK signaling pathway. The MAPK pathway has been shown to be activated in OA, and ERK, a member of the MAPK family, is known to have the ability to disrupt cartilage to promote OA.[43,44] In the riluzole-treated group, the expression of the CTSS, NOS1 and genes in MAPK/ERK signaling pathway was significantly decreased, in addition, as targets of riluzole, CTSS and NOS1 activate the MAPK/ERK signaling pathway. Therefore, we hypothesized that riluzole inhibits the progression of OA by inhibiting the expression of the targets CTSS and NOS1, thus further inhibits the MAPK/ERK signaling pathway. Further in vivo validation is necessary to strengthen the conclusions We propose establishing NOS1 and CTSS knockout zebrafish models using CRISPR/Cas9 technology to examine whether gene knockouts in these pathways protect against OA progression. Additionally, constructing NOS1 and CTSS overexpression zebrafish models could help explore whether these molecules increase OA susceptibility, while also verifying their regulatory effects on the MAPK/ERK signaling pathway.

We have demonstrated the inhibitory effect of riluzole on OA through multiple bioinformatics methods and in vivo experiments, identifying potential targets regulated by riluzole. However, our study has some limitations. First, extracting OB from hard bone tissue is extremely challenging, limiting the amount of publicly available data and the number of successfully isolated samples from our team. Increasing the sample size in future studies would strengthen the credibility of our findings. The femoral heads used in this study were sourced from patients with advanced OA undergoing total hip replacement, and it remains unclear whether similar OB-NE interactions occur in earlier OA stages. Future studies should

investigate the role of these interactions at different stages of OA to better understand the progression of the disease and the potential for drug repurposing. Second, network proximity is a powerful and widely used strategy in drug repositioning, it has important limitations that should not be overlooked. Network-based proximity measures rely heavily on the completeness and accuracy of the underlying interactome and disease module definitions and often consider global network interactions, they may inadvertently prioritize drugs with broad molecular effects and increase the risk of off-target effects. To improve reliability, future studies should integrate complementary drug repositioning strategies, such as transcriptional signature reversal analysis (eg, CMap), alongside network-based approaches. Third, molecular docking and transcriptome analysis indicated that CTSS and NOS1 are potential targets of riluzole, which may exert its effects by regulating the MAPK/ERK pathway. These results provide preliminary evidence for the repurposing of riluzole in OA treatment. However, the causal role of CTSS and NOS1 in OA requires additional verification through subsequent gene interference experiments. Finally, although zebrafish anal fin joints share key features with human cartilage, their simpler bone/immune systems suggest that validation in mammalian models would strengthen the conclusions. Future studies should include OA femoral head samples from different stages to analyze changes in cell communication and assess the efficacy of liraglutide at various stages of OA progression. Despite several other drugs with higher network proximity scores, riluzole was selected due to its established safety profile in ALS treatment and its potential to modulate the CTSS/NOS1-MAPK/ERK pathway, which aligns with the specific mechanisms of OA pathogenesis identified in this study.

Conclusion

This study highlights riluzole as a promising repositioned drug for osteoarthritis by targeting OB-NE interaction, a previously underexplored cellular mechanism in OA pathogenesis. Given riluzole's existing clinical approval for ALS and its well-established safety profile, the findings suggest strong translational potential for OA treatment, pending further preclinical and clinical validation.

Abbreviations

CHON, Chondrocytes; DEGs, Differentially expressed genes; DEX, Dexamethasone; EC, Endothelial cells; eQTLs, Expression quantitative trait locis; ER, Erythrocytes; GO, Gene Ontology; GWAS, genome-wide association study; IVW, Inverse variance weighted; L-R, ligand-receptor; MAC, Macrophages; MACS, Magnetic-Activated Cell Sorting; MR, Mendelian randomization; NE, neutrophils; OA, Osteoarthritis; OB, Osteoblasts; PC, Plasma cells; scDRS, single-cell disease relevance score; scRNA-seq, single-cell RNA sequencing; SMC, Smooth muscle cells; SNPs, Single nucleotide polymorphisms; TCC, Triclocarban; UMAP, Uniform manifold approximation and projection.

Data Sharing Statement

All the datasets could be downloaded directly from the indicated websites. We have uploaded the scRNA seq data of three fracture samples to the GEO database (GSE286109). The three previous scRNA-seq data used in this study can be accessed with accession number of GSE169396.

Consent

All authors approve the manuscript for publication. Written informed consent was obtained from all participants prior to inclusion in the study, confirming their understanding and voluntary agreement with the research protocol.

Funding

There is no funding to report.

Disclosure

The authors have no competing interests in this work.

References

1. Knights AJ, Redding SJ, Maerz T. Inflammation in osteoarthritis: the latest progress and ongoing challenges. *Curr Opin Rheumatol*. 2023;35(2):128–134. doi:10.1097/BOR.0000000000000923
2. Lal JC, Mao C, Zhou Y, et al. Transcriptomics-based network medicine approach identifies metformin as a repurposable drug for atrial fibrillation. *Cell Rep Med*. 2022;3(10):100749. doi:10.1016/j.xcrm.2022.100749
3. Yang L, Tsang KY, Tang HC, Chan D, Cheah KS. Hypertrophic chondrocytes can become osteoblasts and osteocytes in endochondral bone formation. *Proc Natl Acad Sci USA*. 2014;111(33):12097–12102. doi:10.1073/pnas.1302703111
4. Karsdal MA, Bay-Jensen AC, Lories RJ, et al. The coupling of bone and cartilage turnover in osteoarthritis: opportunities for bone antiresorptives and anabolics as potential treatments? *Ann Rheum Dis*. 2014;73(2):336–348. doi:10.1136/annrheumdis-2013-204111
5. Lieben L. Osteoarthritis: osteophyte formation involves PAR2. *Nat Rev Rheumatol*. 2016;12(2):70–71. doi:10.1038/nrrheum.2016.6
6. Wang S, Greenbaum J, Qiu C, et al. Single-cell RNA sequencing reveals in vivo osteoimmunology interactions between the immune and skeletal systems. *Front Endocrinol*. 2023;14:1107511. doi:10.3389/fendo.2023.1107511
7. Guder C, Gravius S, Burger C, Wirtz DC, Schildberg FA. Osteoimmunology: a current update of the interplay between bone and the immune system. *Front Immunol*. 2020;11:58. doi:10.3389/fimmu.2020.00058
8. Salhotra A, Shah HN, Levi B, Longaker MT. Mechanisms of bone development and repair. *Nat Rev Mol Cell Biol*. 2020;21(11):696–711. doi:10.1038/s41580-020-00279-w
9. Trapnell C, Cacchiarelli D, Grimsby J, et al. The dynamics and regulators of cell fate decisions are revealed by pseudotemporal ordering of single cells. *Nat Bbiotechnol*. 2014;32(4):381–386. doi:10.1038/nbt.2859
10. Pliyev BK, Kalintseva MV, Abdulaeva SV, Yarygin KN, Savchenko VG. Neutrophil microparticles modulate cytokine production by natural killer cells. *Cytokine*. 2014;65(2):126–129. doi:10.1016/j.cyto.2013.11.010
11. Benigni G, Dimitrova P, Antonangeli F, et al. CXCR3/CXCL10 axis regulates neutrophil-NK cell cross-talk determining the severity of experimental osteoarthritis. *J Iimmunol*. 2017;198(5):2115–2124. doi:10.4049/jimmunol.1601359
12. Gong Y, Yang J, Li X, et al. A systematic dissection of human primary osteoblasts in vivo at single-cell resolution. *Aging*. 2021;13(16):20629–20650. doi:10.18632/aging.203452
13. Ashburn TT, Thor KB. Drug repositioning: identifying and developing new uses for existing drugs. *Nat Rev Drug Discov*. 2004;3(8):673–683. doi:10.1038/nrd1468
14. Cheng Q, He K, Zhu J, et al. Memantine attenuates the development of osteoarthritis by blocking NMDA receptor mediated calcium overload and chondrocyte senescence. *J Orthop Translat*. 2024;48:204–216. doi:10.1016/j.jot.2024.08.007
15. Blyufer A, Lhamo S, Tam C, Tariq I, Thavornwatanayong T, Mahajan SS. Riluzole: a neuroprotective drug with potential as a novel anti-cancer agent (Review). *Int J Oncol*. 2021;59(5). doi:10.3892/ijo.2021.5275
16. Qiu X, Liu Y, Shen H, et al. Single-cell RNA sequencing of human femoral head in vivo. *Aging*. 2021;13(11):15595–15619. doi:10.18632/aging.203124
17. Hao Y, Hao S, Andersen-Nissen E, et al. Integrated analysis of multimodal single-cell data. *Cell*. 2021;184(13):3573–3587e29. doi:10.1016/j.cell.2021.04.048
18. Korsunsky I, Millard N, Fan J, et al. Fast, sensitive and accurate integration of single-cell data with Harmony. *Nature Methods*. 2019;16(12):1289–1296. doi:10.1038/s41592-019-0619-0
19. Hu C, Li T, Xu Y, et al. CellMarker 2.0: an updated database of manually curated cell markers in human/mouse and web tools based on scRNA-seq data. *Nucleic Acids Res*. 2023;51(D1):D870–D876. doi:10.1093/nar/gkac947
20. Zhang MJ, Hou K, Dey KK, et al. Polygenic enrichment distinguishes disease associations of individual cells in single-cell RNA-seq data. *Nature Genet*. 2022;54(10):1572–1580. doi:10.1038/s41588-022-01167-z
21. de Leeuw CA, Mooij JM, Heskes T, Posthuma D, de Leeuw CA. MAGMA: generalized gene-set analysis of GWAS data. *PLoS Comput Biol*. 2015;11(4):e1004219. doi:10.1371/journal.pcbi.1004219
22. Fang J, Zhang P, Zhou Y, et al. Endophenotype-based in silico network medicine discovery combined with insurance record data mining identifies sildenafil as a candidate drug for Alzheimer's disease. *Nat Aging*. 2021;1(12):1175–1188. doi:10.1038/s43587-021-00138-z
23. Fang J, Zhang P, Wang Q, et al. Artificial intelligence framework identifies candidate targets for drug repurposing in Alzheimer's disease. *Alzheimers Res Ther*. 2022;14(1):7. doi:10.1186/s13195-021-00951-z
24. Zhang Y, He L, Yang Y, et al. Triclocarban triggers osteoarthritis via DNMT1-mediated epigenetic modification and suppression of COL2A in cartilage tissues. *J Hazard Mater*. 2023;447:130747. doi:10.1016/j.jhazmat.2023.130747
25. Chen WC, Lu YC, Kuo SJ, et al. Resistin enhances IL-1beta and TNF-alpha expression in human osteoarthritis synovial fibroblasts by inhibiting miR-149 expression via the MEK and ERK pathways. *FASEB J*. 2020;34(10):13671–13684. doi:10.1096/fj.202001071R
26. Lu W, Shi J, Zhang J, et al. CXCL12/CXCR4 axis regulates aggrecanase activation and cartilage degradation in a post-traumatic osteoarthritis rat model. *Int J Mol Sci*. 2016;17(10):1522. doi:10.3390/ijms17101522
27. Wang X, Cicuttini F, Jin X, et al. Knee effusion-synovitis volume measurement and effects of vitamin D supplementation in patients with knee osteoarthritis. *Osteoarthritis Cartilage*. 2017;25(8):1304–1312. doi:10.1016/j.joca.2017.02.804
28. George J. Vitamin D supplementation and progression of knee osteoarthritis. *JAMA*. 2016;316(3):347–348. doi:10.1001/jama.2016.6314
29. Wang B, Sun W, Bi K, Li Y, Li F. Apremilast prevents IL-17-induced cellular senescence in ATDC5 chondrocytes mediated by SIRT1. *Int J Mol Med*. 2021;47(3). doi:10.3892/ijmm.2021.4845
30. Zhang Y, Huang X, Yuan Y. Anti-inflammatory capacity of Apremilast in human chondrocytes is dependent on SOX-9. *Inflammation Res*. 2020;69(11):1123–1132. doi:10.1007/s00011-020-01392-4
31. Jilka RL. The relevance of mouse models for investigating age-related bone loss in humans. *J Gerontol a Biol Sci Med Sci*. 2013;68(10):1209–1217. doi:10.1093/gerona/glt046
32. Liao Z, Jin Y, Chu Y, et al. Single-cell transcriptome analysis reveals aberrant stromal cells and heterogeneous endothelial cells in alcohol-induced osteonecrosis of the femoral head. *Commun Biol*. 2022;5(1):324. doi:10.1038/s42003-022-03271-6
33. Schieber M, Chandel NS. ROS function in redox signaling and oxidative stress. *Curr Biol*. 2014;24(10):R453–62. doi:10.1016/j.cub.2014.03.034

34. Sha Y, Marshall HE. S-nitrosylation in the regulation of gene transcription. *Biochim Biophys Acta*. 2012;1820(6):701–711. doi:10.1016/j.bbagen.2011.05.008
35. Riegger J, Schoppa A, Ruths L, Haffner-Luntzer M, Ignatius A. Oxidative stress as a key modulator of cell fate decision in osteoarthritis and osteoporosis: a narrative review. *Cell Mol Biol Lett*. 2023;28(1):76. doi:10.1186/s11658-023-00489-y
36. Fischer V, Haffner-Luntzer M. Interaction between bone and immune cells: implications for postmenopausal osteoporosis. *Semin Cell Dev Biol*. 2022;123:14–21. doi:10.1016/j.semcdb.2021.05.014
37. Chakravarti A, Raquil MA, Tessier P, Poubelle PE. Surface RANKL of Toll-like receptor 4-stimulated human neutrophils activates osteoclastic bone resorption. *Blood*. 2009;114(8):1633–1644. doi:10.1182/blood-2008-09-178301
38. Bonnet CS, Gilbert SJ, Blain EJ, Williams AS, Mason DJ. AMPA/kainate glutamate receptor antagonists prevent posttraumatic osteoarthritis. *JCI Insight*. 2020;5(13). doi:10.1172/jci.insight.134055
39. Piepoli T, Mennuni L, Zerbi S, Lanza M, Rovati LC, Caselli G. Glutamate signaling in chondrocytes and the potential involvement of NMDA receptors in cell proliferation and inflammatory gene expression. *Osteoarthritis Cartilage*. 2009;17(8):1076–1083. doi:10.1016/j.joca.2009.02.002
40. Yasuda Y, Kaleta J, Bromme D. The role of cathepsins in osteoporosis and arthritis: rationale for the design of new therapeutics. *Adv Drug Delivery Rev*. 2005;57(7):973–993. doi:10.1016/j.addr.2004.12.013
41. Zhou Y, Liu SQ, Yu L, et al. Berberine prevents nitric oxide-induced rat chondrocyte apoptosis and cartilage degeneration in a rat osteoarthritis model via AMPK and p38 MAPK signaling. *Apoptosis*. 2015;20(9):1187–1199. doi:10.1007/s10495-015-1152-y
42. Bolduc JA, Collins JA, Loeser RF. Reactive oxygen species, aging and articular cartilage homeostasis. *Free Radic Biol Med*. 2019;132:73–82. doi:10.1016/j.freeradbiomed.2018.08.038
43. Loeser RF, Erickson EA, Long DL. Mitogen-activated protein kinases as therapeutic targets in osteoarthritis. *Curr Opin Rheumatol*. 2008;20(5):581–586. doi:10.1097/BOR.0b013e3283090463
44. Lohberger B, Kaltenegger H, Eck N, et al. Shikonin derivatives inhibit inflammation processes and modulate MAPK signaling in human healthy and osteoarthritis chondrocytes. *Int J Mol Sci*. 2022;23(6):3396. doi:10.3390/ijms23063396